Effect of surface protrusion on plasma sheath properties in atmospheric microdischarges

Yangyang Fu,[1,2,a)] Peng Zhang,[2] John P. Verboncoeur,[1,2] Andrew J. Christlieb,[1,2,3] and Xinxin Wang[4]
[1]*Department of Computational Mathematics, Science and Engineering, Michigan State University, East Lansing, Michigan 48824, USA*
[2]*Department of Electrical and Computer Engineering, Michigan State University, East Lansing, Michigan 48824, USA*
[3]*Department of Mathematics, Michigan State University, East Lansing, Michigan 48824, USA*
[4]*Department of Electrical Engineering, Tsinghua University, Beijing 10084, China*

(Received 2 November 2017; accepted 11 January 2018; published online 29 January 2018)

The electric field enhancement due to the presence of cathode surface protrusion is investigated in atmospheric microdischarges with the goal of identifying the plasma sheath properties (such as cathode sheath thickness and electric field distortion). The electric field enhancement caused by surface protrusion is examined by adjusting the aspect ratio and the protrusion size. It is found that the cathode electric field enhancement depends strongly (weakly) on the aspect ratio (size) of the protrusion when it is much smaller than the discharge gap distance. In particular, the axial electric field in both vacuum and discharges becomes nonlinear with the protrusion on the cathode. The cathode sheath thicknesses obtained by two different methods are compared. With the same axial (or radial) protrusion dimension, increasing the aspect ratio will result in a significant decrease in the sheath thickness, whereas increasing the axial protrusion size with an unchanged aspect ratio will only lead to a slight decrease in the sheath thickness. The results contribute to predicting the relative plasma sheath properties from the geometrical parameter of the surface protrusion in atmospheric microdischarges. *Published by AIP Publishing.* https://doi.org/10.1063/1.5011768

I. INTRODUCTION

Microdischarges have received considerable attention because of their wide industrial applications, including plasma display panels (PDPs), ion sources, microelectromechanical systems (MEMS), and microchips.[1–4] These discharges have been investigated by many researchers through experimental diagnostics, analytical methods, and numerical simulations in the past few decades.[5–10] Due to the greatly reduced discharge dimensions, the size of a microdischarge device is usually limited by the basic plasma characteristic length, such as the sheath length or the Debye length. The discharge properties in the micron-scale gaps at high pressure cannot be easily predicted, especially with the presence of the surface roughness and/or surface protrusions on the electrode. In the manufacturing process of the micro-scale gas discharge devices, the roughness or the protrusions on the cathode surface are sometimes inevitable. This greatly affects the plasma discharge properties where the sheath properties (such as sheath thickness) are critical.

Surface protrusion on the electrode usually leads to an electric field enhancement, which has profound effects on the gas breakdowns and high-pressure stable microdischarges. In previous studies, Ang *et al.* analyzed the average electric field enhancement with the presence of a sharp tip in a micron gap through a numerical experiment.[11] A comprehensive analysis of the field distribution and the current emission with the presence of a sharp tip in a finite cathode-anode gap was given by Lin *et al.*[12] Venkattraman investigated the effects of saw-tooth asperity in a channel on the gas breakdown in micro-scale gaps with the field emission mechanism.[13,14] Levko and Raja conducted a fluid modeling of nanosecond pulsed xenon micro-discharge with spherical-protrusion electrodes.[15] It was previously realized that the discharge behavior depends strongly not only on the cathode dimension, the working gas, or the incident power like in the low-pressure cathodes but also on the electrode material, surface roughness, and protrusions.[16,17] As for the steady-state microdischarges at atmospheric pressure, the sheath thickness plays a significant role in the discharge properties, which would be largely affected by the electric field enhancement due to the presence of the surface protrusion. Despite extensive studies in microdischarges, the effects of the surface protrusion (roughness) on the plasma sheath properties are poorly understood, especially in the atmospheric regime.

In order to determine the plasma sheath in microdischarges, Shi and Kong derived a 14% reduction rule on the electric field distribution to define the plasma sheath thickness in both direct-current (DC) and radio-frequency (RF) discharges.[18,19] The 14% rule determines the sheath thickness as the distance between the cathode surface and the spatial position where the cathode electric field is at a magnitude that is 14% of the electric field at the cathode surface. This is in the region near the cathode where a linear electric filed distribution is valid. The 14% rule was validated by Zhang *et al.* in plane-parallel electrode gaps.[20] Following their work, Shi and Kong continued the investigation of the sheath thickness

[a)]Author to whom correspondence should be addressed: fuyangya@egr.msu.edu

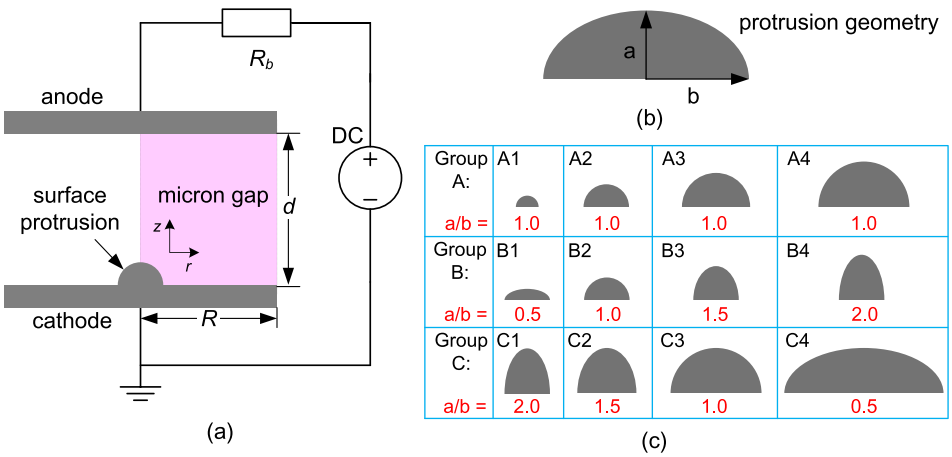

FIG. 1. Schematic of the simulation setup: (a) the micro-discharge gap with an external DC circuit where R_b is the ballast resistor; (b) geometry of the surface protrusion; and (c) three groups (A: A1–A4, B: B1–B4, and C: C1–C4) of the designed protrusions.

in radio-frequency atmospheric micro-plasmas and found that the discharge shows a glow-like plasma structure and the sheath characteristics are independent of the gap size when the electrode gap is significantly greater than the sheath thickness.[21,22] In all these studies, the 14% reduction rule is used in discharges without considering the effect of the surface protrusion.

In this paper, we focus on the effects of the surface protrusion on the cathode plasma sheath properties (mainly on the sheath thickness) in atmospheric microdischarges by a two-dimensional fluid model. The model of a parallel-plate electrode configuration with a relatively small surface protrusion on the cathode is established in argon discharges at atmospheric pressure. The electric field enhancements are investigated by simulations with three groups of different surface protrusions, which are defined with different geometrical sizes and aspect ratios. In Sec. II, the parameters of surface protrusions and the description of the fluid model are given. In Sec. III, the 14% reduction rule and the quasineutrality-based method are used to determine the sheath thickness. The results from the two methods are compared. Also presented are the distributions of the vacuum electric field and the electric field in steady-state discharges. The cathode sheath thicknesses obtained by the two methods are also compared. Finally, concluding remarks are given in Sec. IV.

II. MODEL DESCRIPTION

The schematic of the simulation arrangement is shown in Fig. 1. The configuration of the micro-discharge model with a single surface protrusion on the grounded cathode is shown in Fig. 1(a). A DC voltage is applied on the micron-gap through a ballast resistor R_b of 100 kΩ. The micron-gap length d is 800 μm, and the electrode radius R is 500 μm. In Fig. 1(b), the parameters a and b are used to define the geometry of the surface ellipsoidal protrusion. The aspect ratio a/b can be used to identify the geometry shape. The protrusion will be hemispherical when $a/b = 1.0$ and hemi-ellipsoidal when $a \neq b$. The electric field enhancement and the cathode sheath thickness are investigated for different cases in Fig. 1(c). In group A (A1–A4), the protrusions are all hemispherical and enlarged, keeping $a/b = 1.0$; in group B (B1–B4), the protrusions are enlarged with a/b increasing from 0.5 to 2.0 with b fixed; in group C (C1–C4), the protrusions are enlarged with a/b decreasing from 2.0 to 0.5 with a fixed. The protrusion size is chosen in a range of 25–100 μm which is comparable to the cathode sheath thickness in atmospheric pressure discharges.[18] The protrusion parameters for groups A, B, and C are shown in Table I. The effects of the aspect ratio and protrusion size on the sheath properties can be compared based on these designed cases. In such a way, a dominant impact factor on the electric field enhancement and sheath properties can be identified.

The fluid model of plasma consists of a set of coupled equations, including the species continuity equation, electron energy conservation equation, and Poisson's equation, which are solved self-consistently.[23–25] It was previously employed to investigate the plasma sheath properties in diversified situations.[26–30] The detailed description of the fluid model can be found in our former studies.[31,32] A short description is made here for completeness. Since the present plasma simulations are carried out in a low-temperature (approximate to the room-temperature) region where plasma heating is found to be small, a constant temperature of the heavy particles of 300 K is assumed. The electron emission due to field emission is neglected since the field emission starts to contribute to the total electron emission from the cathode when the electric field becomes on the order of 10^9 V/m or larger.[33–35] In the cases studied here, the magnitude of the cathode electric field (10^6–10^7 V/m) allows us to neglect the field emission processes.

At the cathode boundary, the electric potential is $\varphi = 0$ and the secondary electron emission mechanism due to ion bombardments is included. The normal flux of electrons Γ_e emitted by the cathode is related to the flux of incident ions Γ_i in terms of an effective secondary emission coefficient which is fixed at 0.1.[36,37] Relevant reactions and their

TABLE I. Parameters of the designed protrusions.

Group no.	Parameter	Linear dimension (μm)			
Group A	a	25	50	75	100
	b	25	50	75	100
Group B	a	25	50	75	100
	b	50	50	50	50
Group C	a	100	100	100	100
	b	50	66.7	100	200

coefficients for argon plasma chemistry are taken from Ref. 38. The cross sections of electron impact reactions are originally referred from Biagi database, and the Boltzmann solver (BOLSIG+) is used.[39,40] At the anode boundary, the electric potential is obtained by relation $\varphi = U_0 - I \cdot R_b$. For the boundary at $r = R$, the surface charge density σ_s is specified by $\boldsymbol{n} \cdot \boldsymbol{D} = \sigma_s$, where $\boldsymbol{n}$ is the unit normal vector, $\boldsymbol{D}$ is the electric displacement field, and the balance equation for σ_s is $d\sigma_s/dt = e \cdot (\Gamma_i - \Gamma_e)$.[41] The fluxes of the excited species are changed by the quenching reactions at the boundary surfaces.[42] The equations are solved time-dependently, and the results are obtained when the discharge reaches the steady-state. In the simulation, the gap voltage at the steady-state with different protrusions can be kept constant by adjusting the applied source voltage. To achieve effective comparisons between different cases, the sheath properties are characterized in steady-state discharges with the same gap voltage.

III. RESULTS AND DISCUSSION

Determining the sheath properties near plasma boundaries is a task as old as the discipline of plasma physics.[43,44] Even now, due to the wide range of physical conditions, it is still hard to obtain a universal determination of the critical point of the sheath boundaries.[45,46] For one specific situation, the sheath boundary can still be identified by some feasible methods with limited approximations. Here, we adopt the determination methods of sheath thickness by using the 14% reduction rule and the quasineutrality-based method. According to the theory for a typical DC plasma sheath region, the axial electric field usually decreases linearly, which is widely confirmed by one-dimensional and two-dimensional modeling in discharges in plane-parallel gaps.[42,47] Due to the nonlinear reduction of the electric field near the sheath boundary, the 14% reduction rule is derived to remove the differential effect.[18] The 14% reduction rule can be used when the linear electric filed distribution is valid in the cathode region. However, this linear characteristic of the electric field may not be always valid due to the presence of the surface protrusion on the cathode. In this situation, the 14% reduction rule might be less applicable. On the other hand, considering the inner structure of the plasma sheath, the sheath boundary is the spatial location where the quasineutrality becomes invalid. The plasma sheath thickness can be essentially identified by finding the critical position where the departures from the quasineutrality condition (macroscopic electric neutrality) occur.[44,48]

Figure 2 shows the general effect of surface protrusions on electric potential distributions near the cathode protrusion region ($r \leq 200\,\mu$m and $z \leq 200\,\mu$m) with and without the discharges. Without the surface protrusion, the equipotential lines are in parallel, as shown in Figs. 2(a) and 2(f). In the cases with a surface protrusion, as shown in Figs. 2(b)–2(e) and 2(g)–2(j), the electric equipotential lines are significantly distorted near the protrusion apex, resulting in an enhanced electric field. It can be seen that the shape of the equipotential lines in the gap with and without discharge is quite similar near the cathode surface of a given protrusion. In the discharge with a surface protrusion, the sheath expands radially from the protrusion tip in a nonlinear fashion, as shown in Figs. 2(b)–2(e). The effect of the surface protrusion is gradually smoothed away from the cathode sheath region, which is similar to the result of previous sheath modeling with a rough cathode surface.[49]

Figure 3 shows the axial distributions of the electric field E_{dis} and the charged particle densities (electron density n_e and ion density n_i) in the plane-parallel gap with and without cathode protrusion, respectively. In Fig. 3(a), the electric field decreases linearly in the plane-parallel gap, while in Fig. 3(b), the electric field shows a severe nonlinear distribution with a hemispherical protrusion ($a = 100\,\mu$m) on the cathode. In Fig. 3(a), the 14% rule shows good consistency with the quasineutrality method in identifying the sheath thickness. Here, the condition $n_e = 90\%\ n_i$ is used for the quasineutrality. However, due to the nonlinearity of the electric field, the 14% rule truncates the sheath thickness with an error Δz, as shown in Fig. 3(b). Obviously, this method will lead to an underestimation of the sheath thickness when the electric field drops in a more steep way in the cathode region. Therefore, the quasineutrality method is recommended, while the 14% rule is not well applied when the surface protrusion appears on the cathode.

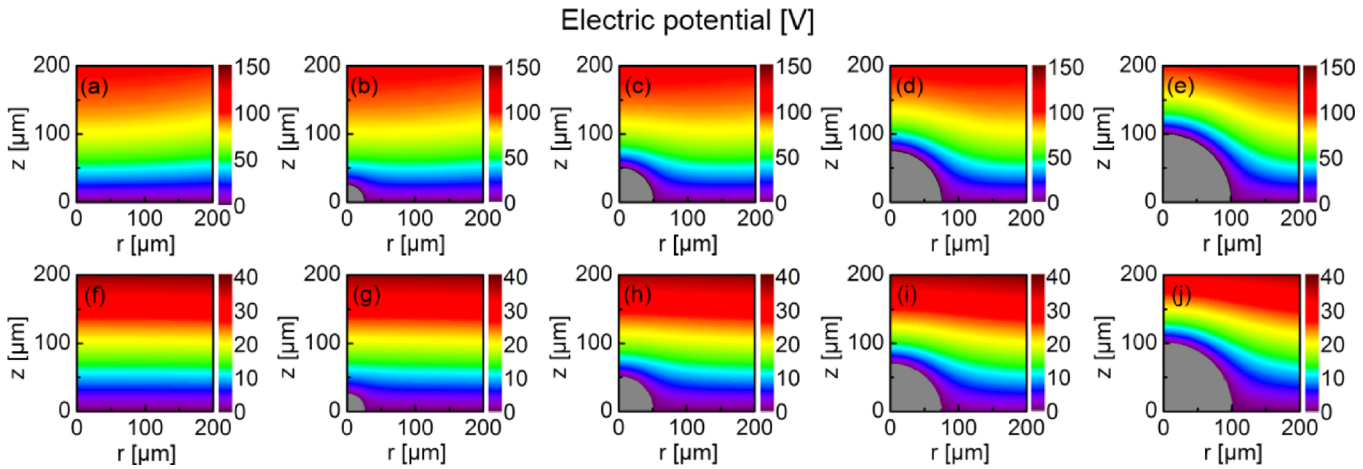

FIG. 2. The electric potential distributions with (top) and without (bottom) discharge near a hemispherical protrusion with $a = b$ from 0 to 100 μm. The gap voltage in cases (a)–(j) is kept at 150 V.

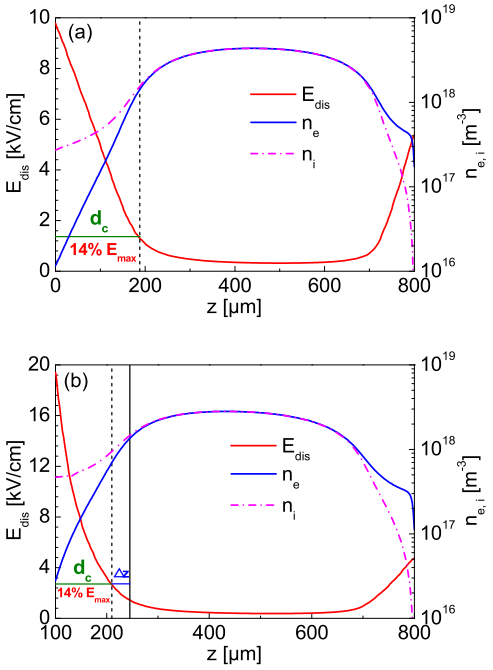

FIG. 3. Determination of the cathode sheath thickness with and without a surface protrusion. (a) Cathode without a protrusion and (b) cathode with a hemispherical protrusion in the 100 μm radius.

Figure 4 shows the axial distributions of the electric field E_v in vacuum and the electric field E_{dis} under steady-state discharges from the protrusion apex to the anode for different radii of protrusions in group A, the hemispherical protrusions ($a = b$) from 25 μm to 100 μm. The electric field distributions are compared to the special case without protrusion ($a = b = 0$). In Fig. 4(a), the enhanced vacuum electric fields on the apex of the protrusion are almost the same, about 5.76 kV/cm, with the gap voltage at 150 V for all the cases. For the cathode without surface protrusion, the vacuum field distribution is nearly uniform and the electric field intensity is about 1.92 kV/cm at the cathode. The vacuum electric field enhancement caused by these hemispherical protrusions is about 3, regardless of the protrusion radius, which also agrees with previous studies.[50,51] In steady-state discharges, due to the presence of space charge effects, the electric field is further distorted from the vacuum electric field. Figure 4(b) shows the electric field enhancement at the apex of the hemispherical protrusion in the steady-state discharge. The maximum electric field gradually decreases from 24.7 kV/cm to 19.3 kV/cm as the axial protrusion size increases from 25 μm to 100 μm. Profiles of the axial electric field distributions are similar but no longer linear. The enhancement of the electric field in both vacuum and discharges is not significantly influenced by the protrusion size.

Figures 5 and 6 show the distributions of the vacuum electric field and electric field in discharges with protrusions from groups B and C on the cathode surface. The aspect ratio of the protrusions changes in both groups B and C. In group B, the aspect ratio a/b increases from 0.5 to 2.0 with b fixed, and in group C, it decreases from 2.0 to 0.5 with a fixed. The larger the aspect ratio, the sharper the protrusion, and likewise, the smaller the aspect ratio, the flatter the protrusion.

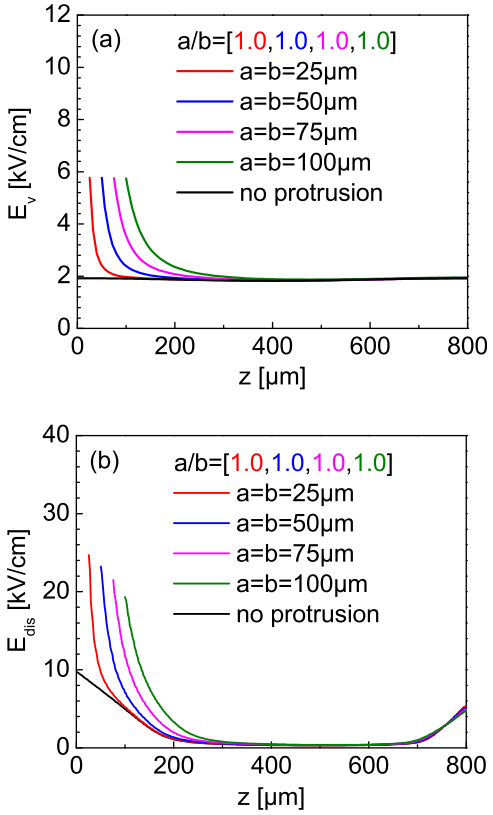

FIG. 4. The axial electric field distributions in gaps with protrusions in group A: (a) the electric field distribution in vacuum E_v and (b) the electric field distribution in discharges E_{dis}. The gap voltage is 150 V for all the cases.

In Figs. 5 and 6, it is observed that the maximum enhanced vacuum electric field increases as the aspect ratio increases. Meanwhile, a similar tendency can be observed in discharges that the maximum enhanced electric field decreases as the aspect ratio decreases. As afore shown in Fig. 4, the maximum enhanced electric field in vacuum is constant in spite of the protrusion size being increased considerably, while the maximum enhanced electric field in discharges decreases slightly when the aspect ratio is fixed. In groups B and C, the tendency of the electric field enhancement is mainly determined by the changing of the aspect ratio. Based on the results in Figs. 4–6, it can be concluded that the distortion of the vacuum electric field is mainly determined by the aspect ratio and is less influenced by the protrusion size. Also, the vacuum field property is correlated with that in the discharge to some degree. In all the cases with protrusions, the electric field shows obvious nonlinear distributions in the cathode region. Also, note that the stronger the electric field enhancement, the more severe the nonlinearity becomes, which might lead to the inconsistency of the sheath thickness predictions from the 14% reduction rule. In the plasma discharges with protrusions in groups A, B, and C, the plasma sheath thickness can be obtained by the 14% reduction criteria based on the electric field profiles in Figs. 4(b), 5(b), and 6(b) and by the quasineutrality method based on the distributions of charged particles.

The sheath thicknesses obtained from the 14% reduction rule and the quasineutrality method are shown in Fig. 7 with a fixed discharge gap voltage at 150 V. The sheath thicknesses

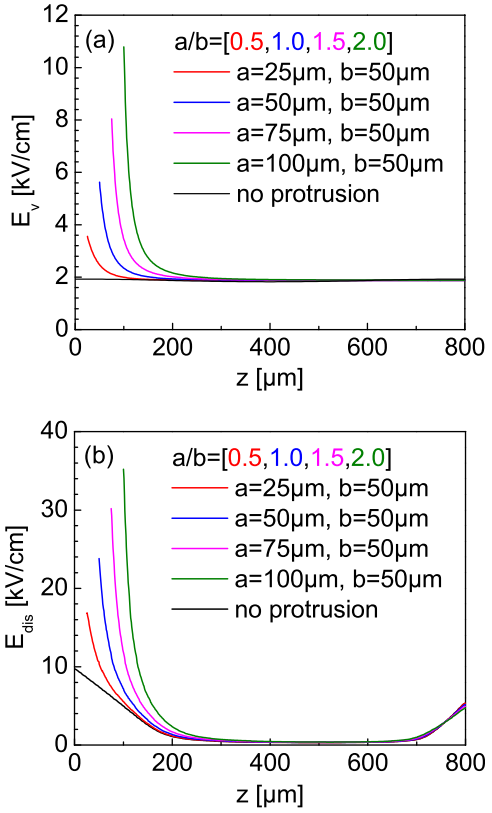

FIG. 5. The axial electric field distributions in gaps with protrusions in group B: (a) the electric field distribution in vacuum E_v and (b) the electric field distribution in discharges E_{dis}. The gap voltage is 150 V for all the cases.

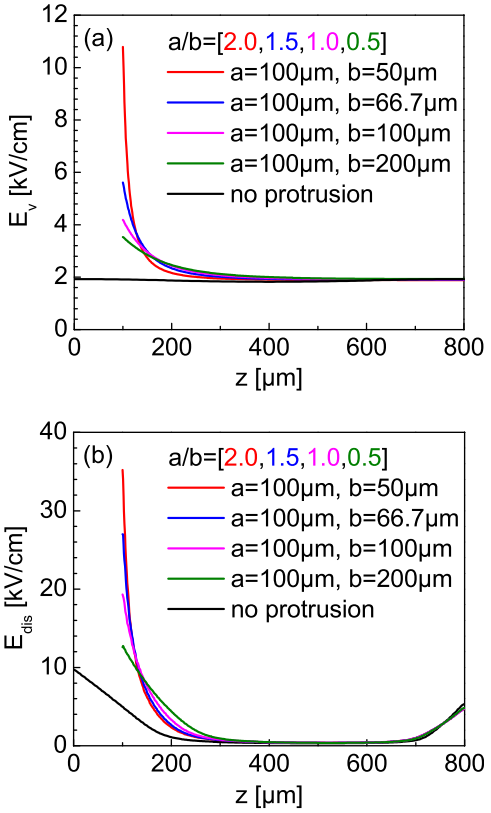

FIG. 6. The axial electric field distributions in gaps with protrusions in group C: (a) the electric field distribution in vacuum E_v and (b) the electric field distribution in discharges E_{dis}. The gap voltage is 150 V for all the cases.

from the 14% reduction rule and from the quasineutrality method are quite different. With the presence of the cathode protrusions, the values of the sheath thicknesses d_c from the 14% rule are lower than those from the quasineutrality method. In Fig. 7(a), for the hemispherical protrusion in group A, when the axial protrusion dimension a increases from 25 to 100 μm with a constant aspect ratio, the sheath thickness decreases at first and then is kept nearly constant, about 140 μm with the quasineutrality method and 100 μm with the 14% rule. This indicates that further increasing the protrusion size may not bring a significant impact on the sheath thickness. In Fig. 7(b), for the protrusions in groups B and C, the sheath thickness decreases with the increase in the a/b ratio from 0.5 to 2.0. Note that, in group B, the radial dimension b is kept the same and the axial dimension a increases from 25 to 100 μm, whereas in group C, the axial dimension a is kept the same and the radial dimension b increases from 25 to 100 μm. It can be observed that, for both groups B and C, the difference between the sheath thicknesses from two different methods is enlarged as the a/b ratio increases. It means that the difference in the sheath thickness from the two methods becomes smaller when the protrusion is flatter. The variation range of the sheath thicknesses caused by the aspect ratio can reach 100 μm with the increase in a/b from 0.5 to 2.0. As for the effect of the protrusion size, taking the protrusion B1 and C4 shown in Fig. 1(c), for example, protrusion C4 is four times as large as protrusion B1. As shown in Fig. 7(b), the difference of the sheath thickness caused by B1 and C4 is only around 20 μm from the 14% reduction rule and even less from the quasineutrality method. This is much less than the difference caused by the aspect ratio, which indicates that the aspect ratio has a more dominant impact on the sheath thickness than the protrusion size.

Based on the discussion above, it can be confirmed that as the protrusion size increases, the smaller a/b ratio will result in a larger sheath thickness; on the other side, the larger a/b ratio will lead to a smaller sheath thickness. The protrusion aspect ratio is identified as the more dominant impact factor on the sheath properties than the protrusion size. Although the sheath thicknesses from the two methods are different, the general tendencies are found to be similar, which are still useful in qualitative predictions. As shown in Figs. 4–6, the tendency of the electric field distributions with and without discharge is similar, and as shown in Fig. 7, the cathode sheath thickness is found to be related to the uniformity of the electric field distribution inside the discharge gap. The tendency of the relative cathode sheath thickness could be generally estimated from the vacuum field and the protrusion geometry parameters. This property is similar to the space-charge-limited (SCL) current flow in vacuum diodes, where the SCL current density can be estimated by only using the cathode vacuum electric field.[52,53] Further simulation shows that the general trends are consistent for different gap voltages.

IV. CONCLUSION

In this work, the effect of a single small surface protrusion on the properties of the cathode plasma sheath in the

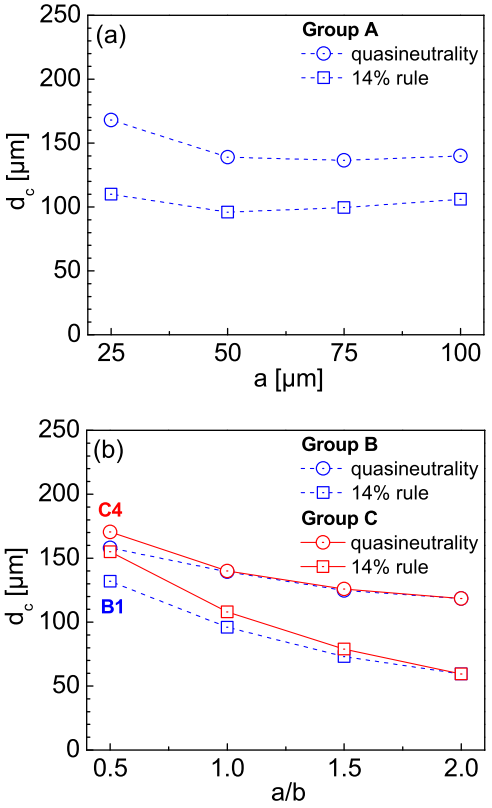

FIG. 7. The dependence of sheath thickness d_c on the protrusion dimension and aspect ratio a/b with a fixed gap voltage at 150 V. (a) Sheath thickness as a function of the protrusion dimension with protrusions in group A and (b) sheath thickness as a function of aspect ratio a/b with protrusions in groups B and C.

atmospheric microdischarges was investigated. The plasma sheath thickness is significantly influenced by the presence of a surface protrusion even though its geometrical size is much smaller than the whole gap. With the protrusion on the cathode surface, both the vacuum electric field and electric field in discharges are largely enhanced and become nonlinear in the cathode region. From the presented cases, it was found that the 14% rule gives lower estimated values of the sheath thickness than those given by the quasineutrality method. The tendencies of the sheath thickness from two methods are similar, and the difference between them is mainly determined by the aspect ratio: the larger aspect ratio, the larger the resulted difference in sheath thickness. When the protrusion is hemispherical (with a constant aspect ratio), as the protrusion size increases, the enhancement of the vacuum field is constant and slightly decreases in the discharge gap. With the same axial (or radial) protrusion dimension, increasing the aspect ratio will lead to an obvious decrease in the sheath thickness, which means that the sheath thickness becomes smaller when the protrusion is sharper. The effect of the protrusion's aspect ratio on the electric field enhancement and the sheath thickness is more significant than that of the protrusion size. The results of this study are beneficial to predict the relative plasma sheath properties from the geometrical parameters of the surface protrusion in atmospheric microdischarges.

ACKNOWLEDGMENTS

This work was supported by the Air Force Office of Scientific Research (AFOSR), the Department of Energy (DOE) Office of Fusion Energy Science, and the DOE Plasma Science Center Grant No. DE-SC0001939. Peng Zhang was supported by AFOSR Grant No. FA9550-14-1-0309 through a subcontract from the University of Michigan and by AFOSR YIP Award No. FA9550-18-1-0061. The authors would also like to thank the National Natural Science Foundation for the support of the research under Contract No. 51777114.

[1]J. P. Boeuf, J. Phys. D: Appl. Phys. **36**, R53 (2003).
[2]J. Franzke, K. Kunze, M. Miclea, and K. Niemax, J. Anal. At. Spectrom. **18**, 802 (2003).
[3]Y. C. Hong and H. S. Uhm, Appl. Phys. Lett. **89**, 221504 (2006).
[4]K. H. Becker, K. H. Schoenbach, and J. G. Eden, J. Phys. D: Appl. Phys. **39**, R55 (2006).
[5]A. Semnani, A. Venkattraman, A. A. Alexeenko, and D. Peroulis, Appl. Phys. Lett. **102**, 174102 (2013).
[6]J. P. Boeuf, L. C. Pitchford, and K. H. Schoenbach, Appl. Phys. Lett. **86**, 071501 (2005).
[7]B. J. Lee, H. Rahaman, I. Petzenhauser, K. Frank, and K. P. Giapis, Appl. Phys. Lett. **90**, 241502 (2007).
[8]K. H. Schoenbach and W. Zhu, IEEE J. Quantum Electron. **48**, 768 (2012).
[9]M. Moselhy, W. Shi, R. H. Stark, and K. H. Schoenbach, Appl. Phys. Lett. **79**, 1240 (2001).
[10]A. M. Loveless and A. L. Garner, IEEE Trans. Plasma Sci. **45**, 574 (2017).
[11]S. Sun and L. K. Ang, J. Appl. Phys. **113**, 144902 (2013).
[12]J. Lin, P. Y. Wong, P. Yang, Y. Y. Lau, W. Tang, and P. Zhang, J. Appl. Phys. **121**, 244301 (2017).
[13]A. Venkattraman, J. Phys. D: Appl. Phys. **47**, 425205 (2014).
[14]A. Venkattraman, Phys. Plasmas **20**, 113505 (2013).
[15]D. Levko and L. L. Raja, Phys. Plasmas **23**, 073513 (2016).
[16]H. Baránková and L. Bárdos, Vacuum **87**, 128 (2013).
[17]M. P. Gomes, B. N. Sismanoglu, and J. Amorim, Braz. J. Phys. **39**, 25 (2009).
[18]J. J. Shi and M. G. Kong, J. Appl. Phys. **94**, 5504 (2003).
[19]J. J. Shi and M. G. Kong, IEEE Trans. Plasma Sci. **33**, 624 (2005).
[20]C. W. Yao, H. C. Ma, Z. S. Chang, P. Li, H. B. Mu, and G. J. Zhang, Acta Phys. Sin. **66**, 025203 (2017).
[21]J. J. Shi and M. G. Kong, Phys. Rev. Lett. **96**, 105009 (2006).
[22]J. J. Shi and M. G. Kong, Appl. Phys. Lett. **87**, 201501 (2005).
[23]E. A. Bogdanov, V. I. Demidov, A. A. Kudryavtsev, and A. I. Saifutdinov, Phys. Plasmas **22**, 024501 (2015).
[24]Y. Fu, H. Luo, X. Zou, and X. Wang, IEEE Trans. Plasma Sci. **42**, 1544 (2014).
[25]P. G. C. Almeida, M. S. Benilov, and M. J. Faria, Plasma Sources Sci. Technol. **19**, 025019 (2010).
[26]U. Shumlak, R. Lilly, N. Reddell, E. Sousa, and B. Srinivasan, Comput. Phys. Commun. **182**, 1767 (2011).
[27]I. Rafatov, E. A. Bogdanov, and A. A. Kudryavtsev, Phys. Plasmas **19**, 093503 (2012).
[28]T. Gyergyek and J. Kovačič, Phys. Plasmas **22**, 043502 (2015).
[29]M. Gohain and P. K. Karmakar, Europhys. Lett. **112**, 45002 (2015).
[30]Y. Fu, H. Luo, X. Zou, and X. Wang, Phys. Plasmas **22**, 023502 (2015).
[31]Y. Fu, H. Luo, X. Zou, and X. Wang, Plasma Sources Sci. Technol. **23**, 065035 (2014).
[32]Y. Fu, J. P. Verboncoeur, A. J. Christlieb, and X. Wang, Phys. Plasmas **24**, 083516 (2017).
[33]A. Venkattraman and A. A. Alexeenko, Phys. Plasmas **19**, 123515 (2012).
[34]Y. Feng and J. P. Verboncoeur, Phys. Plasmas **13**, 073105 (2006).
[35]Y. Feng, J. P. Verboncoeur, and M. C. Lin, Phys. Plasmas **15**, 043301 (2008).
[36]A. Derzsi, I. Korolov, E. Schüngel, Z. Donkó, and J. Schulze, Plasma Sources Sci. Technol. **24**, 034002 (2015).
[37]A. Berkane, S. Rebiai, F. Bouanaka, and H. Bahouh, Phys. Scr. **90**, 065602 (2015).

[38]Y. Fu, J. P. Verboncoeur, and A. J. Christlieb, Phys. Plasmas **24**, 103514 (2017).
[39]See https://fr.lxcat.net for Biagi v8.9 database (retrieved on July 4, 2012).
[40]G. J. M. Hagelaar and L. C. Pitchford, Plasma Sources Sci. Technol. **14**, 722 (2005).
[41]Y. Sakiyama and D. B. Graves, Plasma Sources Sci. Technol. **18**, 025022 (2009).
[42]T. Farouk, B. Farouk, D. Staack, A. Gutsol, and A. Fridman, Plasma Sources Sci. Technol. **15**, 676 (2006).
[43]L. Tonks and I. Langmuir, Phys. Rev. **34**, 876 (1929).
[44]J. E. Allen, Plasma Sources Sci. Technol. **18**, 014004 (2009).
[45]A. V. Godyak and N. Sternberg, IEEE Trans. Plasma Sci. **18**, 159 (1990).
[46]R. N. Franklin, J. Phys. D: Appl. Phys. **36**, R309 (2003).
[47]Y. Fu, H. Luo, X. Zou, K. Liu, and X. Wang, Acta Phys. Sin. **62**, 205209 (2013).
[48]J. A. Bittencourt, *Fundamentals of Plasma Physics* (Springer-Verlag, New York, 2004), p. 279.
[49]See https://www.particleincell.com/starfish/ for examples of Starfish simulations.
[50]J. H. Jeans, *The Mathematical Theory of Electricity and Magnetism* (Cambridge University Press, Cambridge, 1920), p. 194.
[51]P. Zhang, Y. Y. Lau, and R. M. Gilgenbach, J. Appl. Phys. **105**, 114908 (2009).
[52]Y. B. Zhu, P. Zhang, A. Valfells, L. K. R. Ang, and Y. Y. Lau, Phys. Rev. Lett. **110**, 265007 (2013).
[53]P. Zhang, A. Valfells, L. K. Ang, J. W. Luginsland, and Y. Y. Lau, Appl. Phys. Rev. **4**, 011304 (2017).